Journal of Nuclear Materials 547 (2021) 152783

Contents lists available at ScienceDirect

Journal of Nuclear Materials

journal homepage: www.elsevier.com/locate/jnucmat

Small uranium and oxygen interstitial clusters in UO_2: An empirical potential study

X.-Y. Liu*, D.A. Andersson

Materials Science and Technology Division, Los Alamos National Laboratory, Los Alamos, New Mexico 87545, USA

ARTICLE INFO

Article history:
Received 30 September 2020
Revised 18 December 2020
Accepted 4 January 2021
Available online 14 January 2021

Keywords:
Uranium dioxide
Uranium interstitial cluster
Molecular dynamics
Accelerated molecular dynamics
Irradiation induced defects
Defect kinetics

ABSTRACT

The aggregation of defect clusters in UO_2 under irradiations creates dislocation loops and cavities, which in turn contribute to swelling of the fuels, leading to detrimental pellet-clad mechanical interactions. The kinetics of the defect clusters, however, have received less attention and are not well understood. Using two interatomic potentials, the Morelon potential and a many-body model by Cooper, Rushton, and Grimes (CRG), the energetics and kinetics of small uranium interstitial clusters, with and without bound oxygen interstitials, are investigated with molecular dynamics and accelerated molecular dynamics simulations. For the single bound anti-Schottky interstitial cluster (U_i2O_i), both potentials find the interstitialcy migration mechanism to be a low barrier migration mechanism. However, for the CRG potential, an oxygen Frenkel pair assisted interstitial cluster migration mechanism with a lower migration barrier is identified during accelerated molecular dynamics simulations. For the Morelon potential, the interstitial clusters have geometrically compact structures, and small interstitial clusters (two and three anti-Schottky clusters) are more mobile than the single bound anti-Schottky interstitial cluster; for the CRG potential, the interstitial clusters have geometrically non-compact structures, yielding a more complex energy landscape. The rapid migration of interstitials and interstitial clusters are important for the irradiation response of UO_2 and correlates well with the very low barriers reported in a few historic experimental studies.

1. Introduction

Irradiation induced dislocation loops and defect clusters are common features in crystalline materials. Uranium dioxide (UO_2), the most commonly used fuel in light-water nuclear reactors, is no exception. The aggregation of defect clusters in UO_2 results in dislocation loops and cavities, which in turn contributes to the swelling of the fuels, leading to detrimental pellet-clad mechanical interactions. Earlier experimental work by Soullard [1] reported observation of interstitial dislocation loops of ⟨111⟩ type Burgers vector by TEM in UO_2 thin foils irradiated with neutrons. In TEM studies of ion irradiated CeO_2, a surrogate material for UO_2, the faulted loops with Burgers vectors of 1/3⟨111⟩ (Frank loop) lying on {111} planes and consisting of interstitial CeO_2 clusters were observed [2]. In additon, interstitial-type perfect dislocation loops of 1/2⟨110⟩ {110} character were also observed under electron irradiations [3]. More recently, a detailed characterization of dislocations in ion-irradiated polycrystalline UO_2 was carried out [4], which only revealed 1/2⟨110⟩ {110} character dislocation loops.

The kinetics of the defect clusters, which contribute to the growth of dislocation loops, however, have received less attention and are not well understood. In an early review on the topic by Matzke [5], it was noted that upon annealing of self-damaged PuO_2, the damage recovery has a pronounced stage below room temperature. Matzke [5] argued that it seems reasonable to attribute this stage to the metal sublattice, possibly the metal interstitials. In the analysis by Soullard [6], where dislocation loops in UO_2 were obtained by irradiation at room temperature with 1.8 MeV electrons, the estimated migration energy of uranium interstitials was in the range of 0.2 to 0.4 eV, which is extremely low. This analysis was consistent with even earlier experiments showing that interstitial type dislocation loops were observed in reactor irradiated UO_2 at relatively low temperatures, between 50 and 100 °C [7].

Recently, using a combination of experiments and modeling, Chartier et al. [8,9] showed that under irradiation conditions, the early stage faulted Frank loop in UO_2 can be transformed into unfaulted ⟨110⟩ dislocations via addition of Shockley partials. In their molecular dynamics (MD) simulations [8], the Morelon empirical potential was employed, in combination with the Frenkel pair accumulation methodology to minic ballistic damage. While previ-

* Corresponding author.
E-mail address: xyliu@lanl.gov (X.-Y. Liu).

https://doi.org/10.1016/j.jnucmat.2021.152783
0022-3115/

ous modeling studies [8,10–12] have mostly focused on the collision cascade type of MD simulations to understand the dislocation loop generation, in this work, we are interested in understanding the energetics and kinetics of small interstitial clusters that may aggregate to form such dislocation loops. These small interstitial clusters are also considered as basic units in formation of the interstitial dislocation loops. Understanding of interstitial cluster kinetics is also useful for cluster dynamics models, since they may play an important role in controlling the point defect concentrations [13]. It is noted that we are mainly interested in the interstitial cluster behavior under irradiation conditions. In thermal equilibrium the concentration of these clusters will be very small and will not contribute to the total diffusivity, which is rather governed by the mechanisms identified in [14].

Previous density functional theory (DFT) calculations in [15] found that the uranium interstitials in UO_2 migrate by an interstitialcy mechanism in the [100] direction with a barrier of about 4 eV. It is not possible to reconcile the above mentioned experimental measurements based on damage recovery [6], which indicate a few tenths of an eV barrier for uranium interstitials in UO_2, with the DFT result by simply invoking computational uncertainty. It was suggested that the discrepancy may be rooted in the experimental recovery signal corresponding to something other than a single uranium interstitial [14]. Very recently, our DFT study of a bound anti-Schottky defect U_i2O_i [14], i.e. two oxygen interstitials bound to the interstitial uranium ion, revealed that the migration barrier is reduced by $>$ 2 eV compared to a single U_i defect. The interstitial clusters considered in this paper, like the bound anti-Schottky defect, are stoichiometric UO_2 units in interstitial positions. The equilibrium concentration of uranium interstitials is very low and for in-pile conditions uranium interstitials are predominantly expected to be formed by irradiation. It is also expected that oxygen defects, such as oxygen interstitials, are fairly mobile compared to uranium defects [16], and can quickly combine with their uranium interstitial counterpart to form such clusters as well as with sinks, implying that oxygen interstitials may be assumed to be in thermal equilibrium. We only study the U_i2O_i type of clusters, because others do not move as fast and are also less stable [14]. For the remainder of this paper, the single bound anti-Schottky defect cluster is termed as a single uranium interstitial cluster; while multiple stoichiometric UO_2 units in interstitial positions are termed as multiple uranium interstitial clusters, e.g., di- or tri- uranium interstitial clusters.

2. Methods

We use two interatomic potentials to model interstitial defects in UO_2. The first potential is a many-body model developed by Cooper, Rushton, and Grimes (CRG) [17]. The CRG potential utilizes a combined Buckingham-Morse [18,19] and embedded-atom-method (EAM) [20] potential approach. The other potential is developed by Morelon et al. [21]. In the Morelon potential, a piecewise function with four interaction ranges is used to describe the O-O interaction while a Buckingham potential is used to describe the U-O interaction. The parameters of the Morelon potential are taken from [22]. Both potentials have been used before to model interstitial dislocation loops in UO_2 [8,11,13]. Recently, a variable charge many-body potential based on a 2nd moment tight-binding formalism, SMTB-Q potential, has been successfully used to model dislocations (not interstitial dislocation loops) in UO_2 [23]. However, as will be shown later in this paper, we find that the SMTB-Q potential is not suitable for studying uranium interstitial clusters in UO_2.

Most of the simulations employ a $4 \times 4 \times 4$ supercell of cubic UO_2, with a total of 768 atoms. For large interstitial clusters (n UO_2 aggregates, with $n > 3$), the energetics are computed in a supercell oriented along $x = [11\bar{2}]$, $y = [111]$, and $z = [\bar{1}10]$, replicating $4 \times 6 \times 5$ periods of the unit cell along x, y, and z, with a total of 8640 atoms. The choice of this particular supercell shape is made to establish a principal axis with UO_2 oriented in the [111] direction, which is related to the nucleation of Frank loops lying on the {111} plane from the uranium interstitial clusters. We employ the parallel MD code LAMMPS [24] for the simulations, and the particle-particle particle-mesh solver (pppm) implemented in LAMMPS is used to compute the long-range Coulombic interactions. To allow the system to escape any metastable configuration, we subject each interstitial cluster configuration to a thermal anneal at 600 K for 10 ps, maintained using a Langevin thermostat. At the end of the thermal anneal, the system is quenched to 0 K, and then subjected to energy minimization.

The parallel replica dynamics (ParRep) method [25,26] as implemented in the LAMMPS code is used for the accelerated MD simulations. During the accelerated MD simulations, the migration events are tracked. ParRep addresses the timescale limitation of conventional MD simulations for systems with rare events by using multiple replicas of the system to achieve a parallel speedup in the time domain [26]. The supercells are first relaxed by conjugate gradient minimization before they are equilibrated to nearly zero pressure by performing MD simulations for 100 ps at a constant temperature, and then subjected to ParRep simulations. The canonical NVT (constant volume and temperature) ensemble is used for the ParRep simulations. For computational efficiency, the long-range Coulombic interactions are calculated with the Wolf summation method [27].

3. Results

3.1. Basic properties predicted by empirical potentials

The basic properties of UO_2, including the oxygen Frenkel pair formation energy, uranium Frenkel pair formation energy, and Schottky formation energy, are calculated using the empirical potentials. The results are listed in Table 1, in comparison with available experimental data [34] and selected DFT+U results in the literature.

From Table 1, all empirical potentials predict the oxygen Frenkel pair formation energy (E^O_{FP}) reasonably well, as compared to the experimental range of 3.3–4.6 eV. For the uranium Frenkel pair formation energy (E^U_{FP}), both the Morelon and CRG potentials predict values (11.9 and 11.09 eV) fairly close to the DFT value (11.2 eV [15]). However, the tight-binding SMTB-Q potential describes the uranium interstitial poorly [23], predicting a too low value of 5.58 eV, and it is consequently not used further in this work. As pointed out in [23], the failure to capture E^U_{FP} by the SMTB-Q potential roots back to the fitting of short distance core-core pair interactions, not necessarily the advantage of the tight-binding formalism compared to simpler functional forms such as the Morelon or CRG potentials. For the Schottky formation energy, the Morelon potential predicts a lower value (3.9 eV) than the CRG potential (5.05 eV), which is closer to the experimental value (6.5 eV) [5]. Overall, given the empirical nature of interatomic potentials, both the Morelon and CRG potentials predict reasonable defect energetics.

3.2. Single uranium-oxygen interstitial cluster

The single uranium-oxygen interstitial cluster, U_i2O_i, is modeled by placing a uranium interstitial atom at the center of the oxygen cube, which corresponds to the octahedral interstitial position in UO_2. Three different arrangements are considered for the initial positions of the two oxygen interstitials, as shown in Fig. 1. These are positions in (1) the center of nearest neighbor triangles, (2) the parallel edge centers, and (3) the nearby edge centers of

Table 1
The basic properties of UO_2 from empirical potentials, including the oxygen Frenkel pair formation energy (E^O_{FP}), uranium Frenkel pair formation energy (E^U_{FP}), Schottky formation energy (E_{Sch}), and anti-Schottky formation energy ($E_{anti-Sch}$) in comparison with available experimental data and DFT+*U* results. All energies are in eV.

	E^O_{FP}	E^U_{FP}	E_{Sch}	$E_{anti-Sch}$
Morelon pot.	3.0	11.9	3.9	11.9
CRG pot.	4.94	11.09	5.05	10.4
SMTB-Q [23]	4.25	5.58	5.23	-
DFT+*U*	3.83 [28] 4.2 [29]	11.2 [15]	6.45 [28] 6.4 [29]	-
Experiments	3.3 [30] 3.8 ± 0.5 [31] 3.5 ± 0.5 [5] 4.1 [32] 4.6 ± 0.5 [33]	-	6.5 ± 0.5 [5]	-

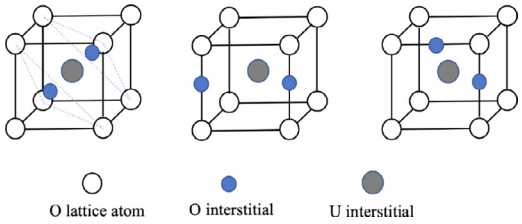

Fig. 1. Schematics illustrating three different options for the oxygen positions in U_i2O_i. The uranium interstitial is placed at the center of the oxygen cube.

Table 2
Comparison of U_i2O_i cluster and U_i migration barriers from empirical potentials to DFT+*U* results. All energies are in eV.

	U_i2O_i	U_i
Morelon pot.	0.98	2.3
CRG pot.	2.3/1.68[a]	3.1
DFT+*U*	1.97 [14]	4.08 [15]

[a] From MD simulations.

oxygen atoms in the cube. Using the CRG potential, the relaxed configurations have formation energies of 29.4, 11.5, and 10.5 eV, respectively. The formation energy of defects is computed using bulk UO_2 as the reference state. However, after thermal annealing, the configurations all relax into the lowest energy configuration, with 10.5 eV in formation energy. This result shows that within the MD procedure, the single uranium interstitial cluster easily reaches the lowest energy state, regardless of its initial starting configuration. A similar result is obtained for the Morelon potential, but with a larger formation energy of 11.9 eV.

In Fig. 2(a)–(f), the migration paths of U_i2O_i obtained using the CRG potential ((a)–(c)) and the Morelon potential ((d)–(f)) are shown. These paths are calculated using the nudged elastic band method with relaxed initial and final configurations. During the exploration of U_i2O_i migration, different possible migration paths/mechanisms are tested. The mechanism shown in Fig. 2 is the interstitialcy mechanism, in which the uranium interstitial atom kicks out a neighboring uranium lattice atom into a vacant octahedral interstitial position, thereby contributing to net diffusion. The oxygen interstitial atoms move with the uranium interstitial during the process. Obviously, this is a complicated multi-step mechanism, thus multiple NEB runs are carried out to determine the migration barriers. The rate-limiting migration energies are 2.3 eV in the CRG case, and 0.98 eV in the Morelon case. These values, together with U_i migration barriers, are listed in Table 2, which also includes DFT+*U* values for comparison.

The final configurations in the migration step are rotated 90 degrees compared to the initial configurations in Fig. 2, for both the CRG and Morelon potentials. The only difference between the rotated and un-rotated configurations is from the position of the oxygen atoms. With the CRG potential, the rotation occurs during annealing at 600 K for 10 ps, indicating a low energy barrier. An additional NEB run is carried out to determine the migration energy between the rotated and un-rotated configurations. The NEB run reveals a small energy barrier of 0.13 eV. Another surprising result from the NEB run is that an additional, even lower energy configuration, is identified, by a tiny energy difference of 0.07 eV along the transition pathway. This configuration did not appear in the direct relaxations from the initial positions. It also did not appear in subsequent MD runs, possibly for entropy reasons. In any case, the tiny energy difference between the lowest energy structure and the assumed initial structure does not change the dominant migration mechanism and only has a minor impact on the effective migration barrier. One important observation from the above result is that, migration of the oxygen atoms associated with the uranium interstitial atom only involves low energy barriers.

From Table 2, it is clear that both the CRG and Morelon potentials predict a substantially reduced migration barrier of U_i2O_i compared to the U_i defect. This is in good agreement with DFT+*U* [14]. In particular, the CRG potential predicts a barrier of 2.3 eV for U_i2O_i, which is closer to the 1.97 eV predicted by DFT+*U* [14] than the 0.98 eV predicted by the Morelon potential.

3.3. Energetics of uranium interstitial clusters

To understand the energetics of uranium interstitial clusters consisting of multiple units, a “misfit” approach is used, as shown in Fig. 3. This was previously used for studying of CeO_2 interstitial clusters by Miao et al. [35]. In this approach, the initial clusters are laid on one of the {111} planes in UO_2. This could be used to mimic the early stage circular $1/3\langle 111\rangle$ dislocation Frank loop, see Fig. 3. This approach has also been used for studying the elastic properties of uranium interstitial clusters in UO_2 [13].

Once the clusters are relaxed and the total energies are obtained, the average formation energy of each cluster can be computed. This is defined as

$$\Delta E^f_n = \frac{E_{cluster} - E_{bulk} - nE_{UO_2}}{n} \quad (1)$$

where n is the number of U_i2O_i clusters, $E_{cluster}$ is the total energy of the supercell, E_{bulk} is the energy of the supercell without cluster defects, and E_{UO_2} is the energy of UO_2 per formula unit (1 U and 2 O atoms). In addition, the average binding energy of each uranium interstitial cluster can be computed. The average binding energy gives a measure of the cluster energy when compared to each isolated U_i2O_i cluster, averaged over the number of clusters,

$$\Delta E^b_n = \frac{n(\Delta E^f_{n=1} - \Delta E^f_n)}{n-1} \quad (2)$$

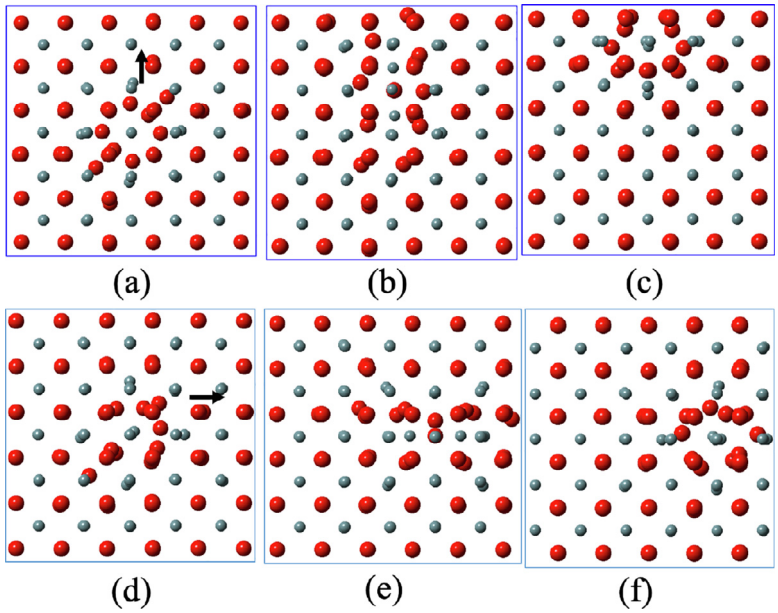

Fig. 2. (a)–(c) The migration path of U_i2O_i using the CRG potential. (d)–(f) The migration path using the Morelon potential. The dark grey spheres are uranium atoms and the red spheres are oxygen atoms. The arrows are used to indicate the migration directions.

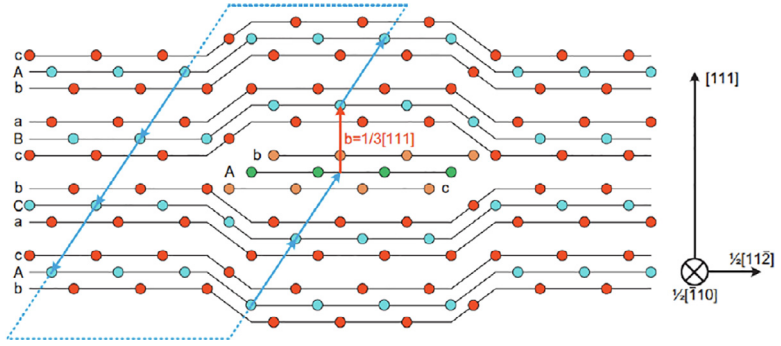

Fig. 3. A schematic illustrating the "misfit" approach from Miao et al. [35]. Reproduced with permission.

Here, a positive binding energy means the clusters attract each other.

As shown in Fig. 4a–c, the formation energies of the UO_2 interstitial clusters follow a monotonic decreasing trend as the cluster size becomes larger (up to 69) for both empirical potentials. However, for the average binding energies of these clusters, there is substantial difference between the CRG potential and the Morelon potential. The Morelon potential result shows a monotonic increasing trend as the cluster size becomes larger, while the CRG potential predicts non-monotonic behavior for cluster sizes of 2, 3, and 6.

In Fig. 4b–c, the binding energies of adding one additional U_i2O_i cluster for cluster sizes of 1, 2, 3, and 18 are also shown. This energy term is defined as,

$$\Delta E^b(n-1,n) = E^{n-1}_{cluster} + E^{n=1}_{cluster} - E^{n}_{cluster} - E_{bulk} \quad (3)$$

For clusters of sizes 3 and 18, different possible adding sites close to the existing cluster were considered. The spread of the scattered binding energy result for these clusters reflects the dependence on the specific sites chosen to add the additional U_i2O_i cluster. The positive binding energy values as shown in Fig. 4b–c indicate that both interatomic potentials favour the creation of size n cluster by addition of another U_i2O_i cluster to size $n-1$ cluster.

This more complex behavior of the binding energies for very small interstitial clusters using the CRG potential is also reflected in the detailed energetics of di-interstitials as a function of the U_i-U_i distance. In Fig. 5, the relative energies of various di-interstitial cluster configurations obtained using the CRG potential are shown as a function of the U_i-U_i distance. Detailed atomic configurations of points *a-e* on the figure are shown as subpanels. The reference energy is a pair of single interstitials separated by infinite distance. The di-interstitial cluster has the lowest energy when the two U_is are in 2nd nearest neighbor (NN) position (point *b*), which is slightly lower in energy than that in 1st NN (point *a*) or 3rd NN cases (point *c*). In contrast, for the Morelon potential, the di-interstitial cluster has the lowest energy when the two single clusters are located next to each other (1st NN, not shown). In general, we find that for the Morelon potential, the predicted interstitial clusters consist of multiple single clusters located next to each other in 1st NN positions, resulting in a geometrically truly compact (closest packed) cluster shape. For the CRG potential, the predicted interstitial clusters consist of multiple single clusters not always located next to each other in 1st NN positions, e.g., in 2nd NN positions, resulting in a geometrically non-compact cluster shape.

Further, when the two U_is are farther apart, the CRG potential predicts that the di-interstitial is a combination of a cuboctahedral (COT) cluster, in which 4 extra O (interstitial) ions surround one U interstitial, and a cluster with no extra O (interstitial) ions. This is highlighted by the case where the U_i-U_i distance at the 7th NN position, where the COT cluster is more than 1 eV lower than two

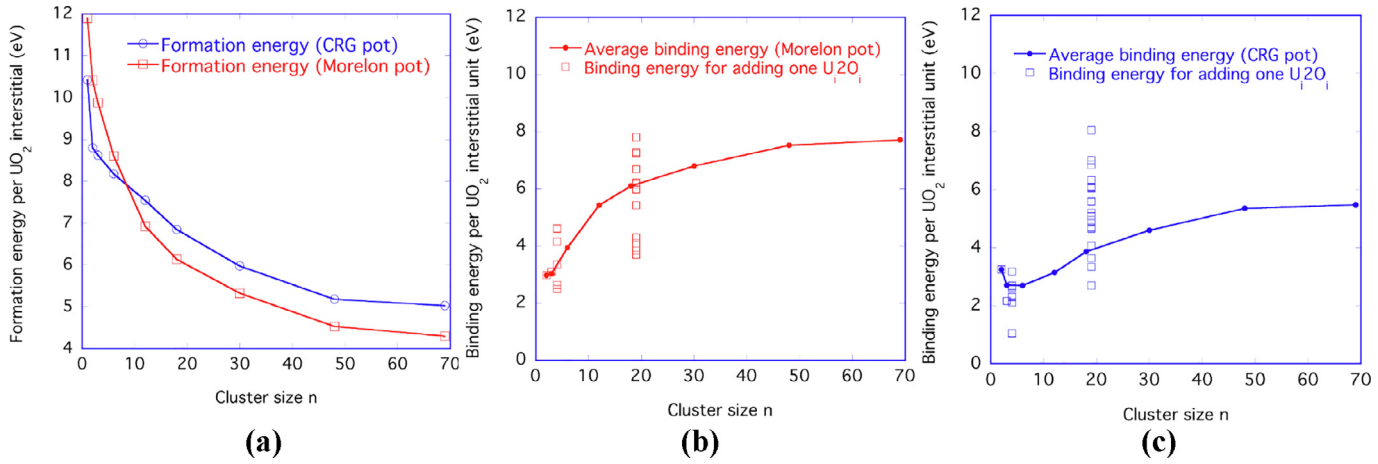

Fig. 4. (a) The average formation energy of uranium interstitial clusters from the CRG and the Morelon potentials as a function of the cluster size n. (b) The average binding energy and the binding energy for adding one additional U_i2O_i cluster from the Morelon potential. (c) The average binding energy and the binding energy for adding one additional U_i2O_i cluster from the CRG potential.

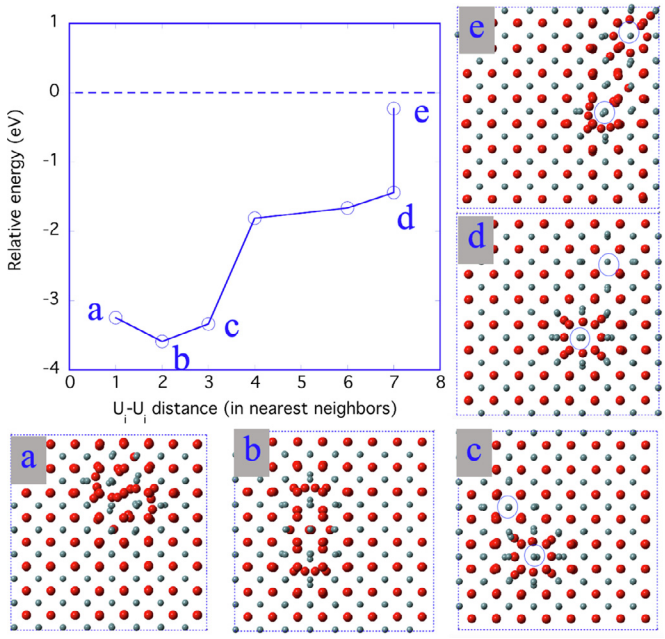

Fig. 5. Upper left: The relative energies of different di-interstitial clusters as a function of the U_i-U_i distance measured in units of nearest neighbors in perfect UO_2, obtained using the CRG potential. The dashed line at zero indicates the reference energy where two single interstitials are separated by infinite distance. The detailed atomic configurations of points a–e on the figure are illustrated in the subpanels surrounding the plot, with uranium interstitials in some configurations singled out by small highlighted circles.

"regular" U_i2O_i clusters separated at the 7th NN position. The COT cluster was observed to form in the low-temperature CeO_2 MD simulations by Aidhy et al [10], but not in their UO_2 MD simulations. Apparently, formation of the COT cluster is closely related to the interatomic potential used. The COT cluster was not observed in the simulations using the Morelon potential.

3.4. Accelerated MD simulations of uranium cluster migration

3.4.1. Morelon potential simulations

Next, we focus on the accelerated MD ParRep simulations for the kinetics of small UO_2 interstitial clusters using the Morelon potential. The temperatures of the ParRep simulations are at 1300, 1600, and 1900 K for the single interstitial cluster, 1300, 1600, and 1900 K for di-interstitial cluster, and 1000, 1300, and 1600 K for tri-interstitial cluster. The choice of temperatures in the ParRep simulations is based on achieving statistically meaningful number of migration events within a reasonable computational time. During the ParRep simulations, the jump distance for each defect migration event is not always the same, which is typical for complicated clusters, thus, we choose to report the migration event time (the average waiting time between migration events) only, similar to our recent work [36]. In Fig. 6a, the averaged times for a migration event to occur during the ParRep simulations for single, di-, and tri-interstitial clusters are shown. Clearly, both the di- and tri-interstitial clusters need much less time for migration events to take place.

The average migration event time t_0 can be fitted to an Arrhenius expression to obtain the cluster migration energy E_m through the following relation [37],

$$\frac{1}{t_0} = \nu_0 e^{-\frac{E_m}{k_B T}}, \tag{4}$$

where k_B is the Boltzmann constant, T is the temperature in K, and ν_0 is a temperature independent prefactor. For the single interstitial cluster, the effective migration energy from the ParRep simulations is determined to be 1.05 eV, closely matching to the migration barrier of 0.98 eV that is determined from the NEB calculations above. The effective migration energies (0.78 eV for di-interstitials and 0.47 eV for tri-interstitials) of multi-interstitial clusters are much lower than the migration barrier in the single interstitial case. NEB studies of interstitial clusters that consist of multiple interstitials are not carried out, because it is much more difficult to identify the relevant mechanism in NEB calculations for complicated clusters consisting of multiple interstitials.

To further investigate this phenomenon, a single interstitial cluster is placed nearby a tri-interstitial cluster, followed by NVT MD simulations at 1000 K. In Fig. 7, a snapshot of the MD simulation is captured showing that the tri-interstitial cluster migrates towards the single interstitial cluster before it finally combines with the single interstitial cluster to form a four-interstitial cluster. This further proves the rapid migration of the tri-interstitial cluster. To quantify the migration of uranium clusters, a displacement analysis is carried out for the configurations during the MD simulation. The analysis is performed using the center of mass of each individual defect cluster (as defined by the uranium atoms only). In Fig. 8, the result for the movement of the tri-interstitial cluster is shown. The single interstitial cluster is essentially not moving during the MD simulation and is not shown in the displacement

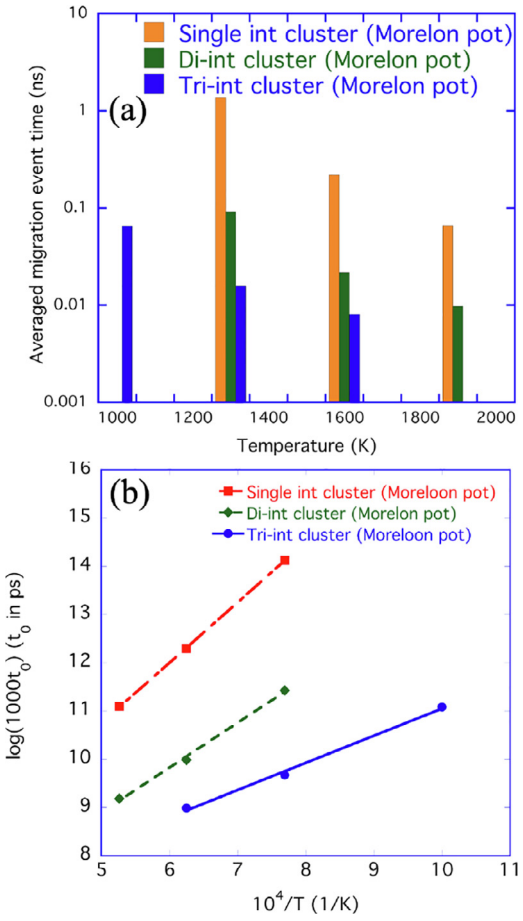

Fig. 6. The averaged time for migration events during MD simulations at different temperatures T for single, di-, and tri-interstitial clusters using the Morelon potential. (b) The migration event time as a function of 1/T. The solid lines are fitted to the Arrhenius expression.

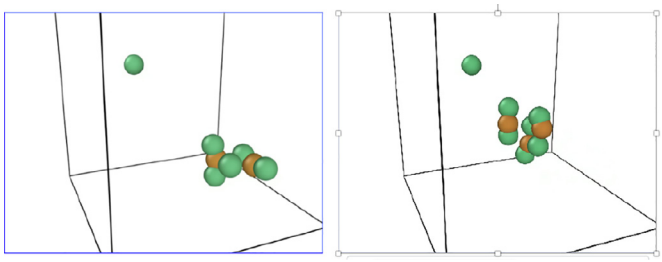

Fig. 7. Snapshots during an MD simulation of a single interstitial cluster nearby a tri-interstitial cluster. Left figure is the starting configuration. For clarity, only uranium defect atoms associated with the clusters are shown, with green atoms as uranium interstitials and brown atoms as uranium vacancies. The defect atoms are identified using an algorithm enabling comparison between the defective supercell and bulk UO_2, as performed similarly in our recent work [36]. In such analysis, a split uranium interstitial is marked as two uranium interstitial atoms plus one uranium vacancy. (For interpretation of the references to color in this figure legend, the reader is referred to the web version of this article.)

figure. The tri-interstitial cluster moves mostly in the x direction, with some motion in the z direction as well.

Finally, a series of single UO_2 interstitial clusters are randomly introduced into bulk UO_2 in a sequential way during MD simulations at 2000 K. For each new introduction of a single UO_2 interstitial cluster into the system, MD simulations are carried out for 100 ps; however, the last MD simulation run could last as long as 1 ns to detect if there is any morphology change in the aggregated

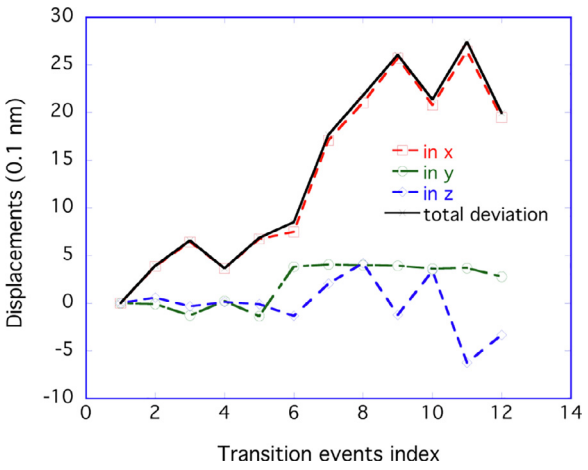

Fig. 8. Displacements of the center of mass of the tri-interstitial cluster in *x*, *y*, *z* and the total displacement as a function of transition event index during the MD simulation in Fig. 7.

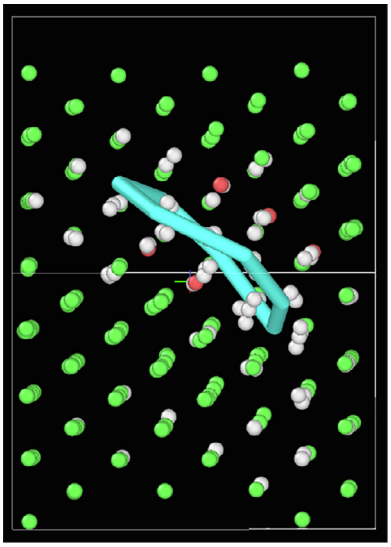

Fig. 9. MD simulation showing the formation of a 1/3⟨111⟩ Frank loop from 10 interstitial clusters. Atoms are colored by common neighbor analysis (CNA) and the dislocation line is extracted using dislocation extraction algorithm (DXA) from Ovito [38].

cluster. In Fig. 9, 1/3⟨111⟩ Frank loop is shown to form when 10 interstitial clusters are introduced into the supercell.

3.4.2. CRG potential simulations

The ParRep simulations using the CRG potential are carried out for single and tri-interstitial clusters. The di-interstitial cluster is not studied due to its complicated behavior stated in Section 3.3. The temperatures of the ParRep simulations ranges from 1400 to 2200 K for both the single interstitial cluster and the tri-interstitial cluster. The slightly higher simulation temperatures used in the ParRep simulations for the CRG potential are intended to reduce the simulation time for generating a meaningful statistical number of events, since the migration barriers are expected to be higher than in the case of the Morelon potential. Precautions are also taken to make sure the temperatures in the ParRep simulations stay below the temperature where the oxygen sublattice premelting is known to occur, at approximately 2500 K [39].

The average time for a migration event to occur during the ParRep simulations as a function of temperature, is shown in Fig. 10. For each cluster case, the result can be split into two temperature

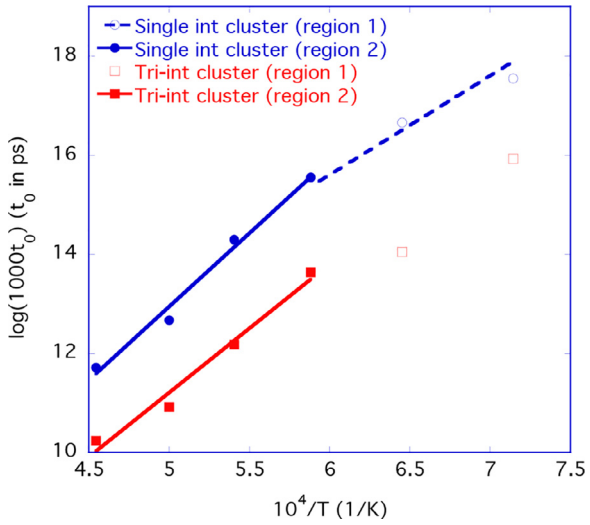

Fig. 10. The migration event time as a function of 1/T. The solid lines are fitted to Arrhenius expressions. The dashed line represents a migration energy of 1.68 eV.

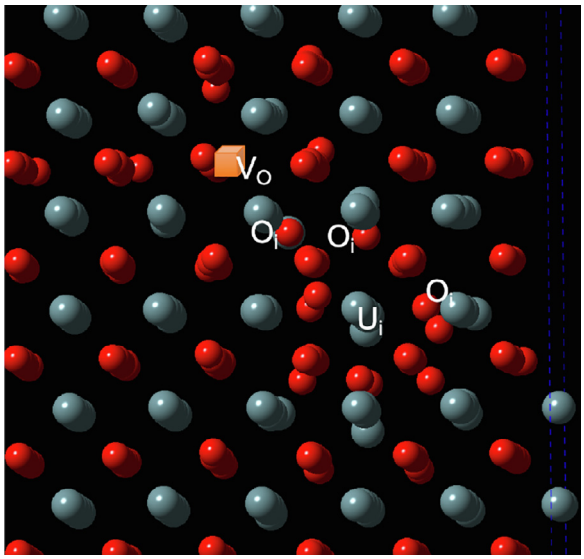

Fig. 11. The configuration of a migrating U_i2O_i cluster assisted by a nearby oxygen Frenkel pair defect. The grey spheres are uranium atoms and the red spheres are oxygen atoms. The orange square indicates an oxygen vacancy. (For interpretation of the references to color in this figure legend, the reader is referred to the web version of this article.)

regimes. Region 1 is from 1400 – 1700 K and region 2 from 1700 – 2200 K. In all cases, the tri-interstitial cluster migrates faster than the single interstitial cluster. For both cases, the data in the higher temperature region approximately follows an Arrhenius relation. Fitting of the migration event time for the single interstitial cluster in region 2 leads to an effective migration energy of 2.5 eV, slightly larger than the value of 2.3 eV obtained from static calculations. For the tri-intersititial cluster, fitting in region 2 leads to a smaller value of 2.2 eV. The fitting is not carried out for data in region 1, due to the large variation caused by fewer statistical events at 1400K.

From the MD simulations of the single interstitial cluster, a different mechanism than that found earlier is revealed. The new mechanism is assisted by an oxygen Frenkel pair nearby the U_i2O_i cluster, with a migration energy somewhat lower than the interstitialcy mechanism identified by static calculations, 1.68 eV instead of 2.3 eV. The configuration involved in the new mechanism is shown in Fig. 11. The new configuration with the bound interstitial U_i3O_i + V_O is less stable than the U_i2O_i cluster. It is close to the saddle energy point along the migration path, 1.6 eV higher than the U_i2O_i configuration. After the migration event, the O vacancy disappears by recombination with the O interstitial. We suspect that both migration mechanisms might contribute to the diffusivity. Indeed, as shown in Fig. 10, the turning point of different Arrhenius behavior occurs at 1700 K, with the lower temperature region with tendency for lower migration energy.

4. Discussion

It is interesting to note that in general, the small interstitial clusters examined in this work migrate faster than the single interstitial cluster. It is also well known that the interstitial clusters in metals sometimes diffuse rapidly, i.e., in bcc iron [40].

The CRG potential predicts the migration barrier for single interstitial cluster in good agreement with DFT. The geometrically non-compact cluster shape for di- and tri- interstitial clusters from the CRG potential simulations suggests a complex energy landscape associated with the clusters. We did not try to confirm this aspect from DFT due to the large size of the computational supercells. For the Morelon potential, the interstitial clusters have more compact structures. This reflects the robustness of the Morelon potential in modeling uranium interstitial clusters, and the associated uranium interstitial dislocation loops, as has been demonstrated in other recent works [8,11,13]. However, the Morelon potential predicts too low migration barrier for the single interstitial cluster (U_i2O_i) compared to DFT, thus, it is not ideal for studying the kinetics of uranium interstitial clusters in a quantitative way. However, we still believe that the qualitative systematic trends are reliable.

5. Conclusions

In this work, the energetics and kinetics of small uranium interstitial clusters which are the bound anti-Schottky defects in interstitial positions, have been investigated using two interatomic potentials for UO_2, i.e., the Morelon and the CRG potentials. Both MD and accelerated MD simulations using the ParRep method are carried out. The following conclusions are obtained:

(1) The interstitialcy migration mechanism for the single interstitial cluster, i.e. a uranium interstitial with two oxygen interstitials, has a migration barrier of 0.98 eV and 2.3 eV for the Morelon and the CRG potentials, respectively, with the latter in close agreement with the DFT + *U* value of 1.97 eV. However, for the CRG potential, an oxygen Frenkel pair assisted single interstitial cluster migration mechanism with a lower migration barrier of 1.68 eV is identified in the accelerated MD simulations.

(2) The formation energies of the UO_2 interstitial clusters follow a monotonic decreasing trend as the cluster size becomes larger. This suggests that it is energetically favorable for clusters to aggregate together.

(3) Small interstitial clusters such as di- and tri-interstitials have faster migration mechanisms than the single interstitial cluster.

(4) For the Morelon potential, the small interstitial clusters have geometrically compact structures while for the CRG potential, the small interstitial clusters have geometrically less compact structures, yielding a more complex energy landscape.

(5) Small interstitial clusters can grow into $1/3\langle 111\rangle$ faulted Frank loop for a relatively small number of clusters aggregated together, e.g., a size of 10.

Declaration of Competing Interest

The authors declare that they have no known competing financial interests or personal relationships that could have appeared to influence the work reported in this paper.

CRediT authorship contribution statement

X.-Y. Liu: Conceptualization, Investigation, Writing - original draft, Visualization, Project administration, Writing - review & editing. **D.A. Andersson:** Conceptualization, Project administration, Writing - review & editing, Funding acquisition.

Acknowledgements

We thank Blas Uberuaga and Danny Perez for helpful discussions. This material is based upon work supported by the U.S. Department of Energy Office of Science, Office of Advanced Scientific Computing Research, and Office of Nuclear Energy, through the Scientific Discovery through Advanced Computing (SciDAC) program. Los Alamos National Laboratory (LANL) is operated by Triad National Security, LLC, for the National Nuclear Security Administration of the U.S. Department of Energy under Contract No. 89233218CNA000001.

References

[1] J. Soullard, Mise en evidence de boucles de dislocation imparfaites dans des echantillons de bioxyde d'uranium irradies, J. Nucl. Mater. 78 (1978) 125.
[2] W.-Y. Chen, J. Wen, M. Kirk, Y. Miao, B. Ye, B. Kleinfeldt, A. Oaks, J. Stubbins, Characterization of dislocation loops in CeO_2 irradiated with high energy Krypton and Xenon, Phil. Mag. 36 (2013) 4569.
[3] K. Yasunaga, K. Yasuda, S. Matsumura, T. Sonoda, Electron energy-dependent formation of dislocation loops in CeO_2, Nucl. Instr. Meth. Phys. Res. B 266 (2008) 2877.
[4] C. Onofri, M. Legros, J. Léchelle, H. Palancher, C. Baumier, C. Bachelet, C. Sabathier, Full characterization of dislocations in ion-irradiated polycrystalline UO_2, J. Nucl. Mater. 494 (2017) 252.
[5] H. Matzke, Atomic transport properties in UO_2 and mixed oxides (U, Pu)O_2, J. Chem. Soc. Faraday Trans. 2 (1987) 1121.
[6] J. Soullard, High voltage electron microscope observations of UO_2, J. Nucl. Mater. 135 (1985) 190.
[7] A.D. Whapham, B.E. Sheldon, Radiation damage in uranium dioxide, Philo. Mag. 12 (1965) 1179.
[8] A. Chartier, L.V. Brutzel, C. Sabathier, O. Dorosh, J. Jagielski, Early stages of irradiation induced dislocations in urania, Appl. Phys. Lett. 109 (2016) 181902.
[9] A. Debelle, J.-P. Crocombette, A. Boulle, A. Chartier, T. Jourdan, S. Pellegrino, D. Bachiller-Perea, D. Carpentier, J. Channagiri, T.-H. Nguyen, F. Garrido, L. Thomé, Lattice strain in irradiated materials unveils a prevalent defect evolution mechanism, Phys. Rev. Mater. 2 (2018) 013604.
[10] D. Aidhy, D. Wolf, A. El-Azab, Comparison of point-defect clustering in irradiated CeO_2 and UO_2: A unified view from molecular dynamics simulations and experiments, Scripta Mater. 65 (2011) 867.
[11] H. Balboa, L.V. Brutzel, A. Chartier, Y.L. Bouar, Damage characterization of (U,Pu)O_2 under irradiation by molecular dynamics simulations, J. Nucl. Mater. 512 (2018) 440.
[12] G. Martin, P. Garcia, C. Sabathier, L.V. Brutzel, B. Dorado, F. Garrido, S. Maillard, Irradiation-induced heterogeneous nucleation in uranium dioxide, Phys. Lett. 374 (2010) 3038.
[13] A.L. Prioux, P. Fossati, S. Maillard, T. Jourdan, P. Maugis, Empirical potential simulations of interstitial dislocation loops in uranium dioxide, J. Nucl. Mater. 479 (2016) 576.
[14] C. Matthews, R. Perriot, M.W. Cooper, C.R. Stanek, D.A. Andersson, Cluster dynamics simulation of uranium self-diffusion during irradiation in UO_2, J. Nucl. Mater. 527 (2019) 151787.
[15] B. Dorado, D.A. Andersson, C.R. Stanek, M. Bertolus, B.P. Uberuaga, G. Martin, M. Freyss, P. Garcia, First-principles calculations of uranium diffusion in uranium dioxide, Phys. Rev. B 86 (2012) 035110.
[16] H. Matzke, Atomic mechanisms of mass transport in ceramic nuclear fuel materials, J. Chem. Soc. Faraday Trans. 86 (1990) 1243–1256.
[17] M.W.D. Cooper, M.J.D. Rushton, R.W. Grimes, A many-body potential approach to modelling the thermomechanical properties of actinide oxides, J. Phys. Condens. Matter. 26 (2014) 105401.
[18] R.A. Buckingham, The classical equation of state of gaseous helium, neon and argon, Proc. Roy. Soc. Lond. Ser. A Math. Phys. Sci. 168 (1938) 264.
[19] P.M. Morse, Diatomic Molecules According to the Wave Mechanics. II. Vibrational Levels, Phys. Rev. B 34 (1929) 57.
[20] M.S. Daw, M.I. Baskes, Embedded-atom method: Derivation and application to impurities, surfaces, and other defects in metals, Phys. Rev. B 29 (1984) 6443.
[21] N.-D. Morelon, D. Ghaleb, J.-M. Delaye, L. Brutzel, A new empirical potential for simulating the formation of defects and their mobility in uranium dioxide, Philos. Mag. 83 (2003) 1533–1550.
[22] X.-Y. Liu, E. Martinez, B. Uberuaga, Dissociated vacancies and screw dislocations in MgO and UO_2: atomistic modeling and linear elasticity analysis, Sci. Reps. 9 (2019) 6499.
[23] A. Soulie, J.-P. Crocombette, A. Kraych, F. Garrido, G. Sattonnay, E. Clouet, Atomistically-informed thermal glide model for edge dislocations in uranium dioxide, Acta Mater. 150 (2018) 248–261.
[24] S. Plimpton, Fast parallel algorithms for short-range molecular dynamics, J. Comput. Phys. 117 (1) (1995) 1–19.
[25] A. Voter, Parallel replica method for dynamics of infrequent events, Phys. Rev. B 57 (1998) R13985.
[26] D. Perez, B. Uberuaga, A. Voter, The parallel replica dynamics method – Coming of age, Comput. Mater. Sci. 100 (2015) 90.
[27] D. Wolf, P. Keblinski, S.R. Phillpot, J. Eggebrecht, Exact method for the simulation of Coulombic systems by spherically truncated, pairwise r^{-1} summation, J. Chem. Phys. 110 (1999) 8254.
[28] R. Perriot, C. Matthews, M. Cooper, B. Uberuaga, C. Stanek, D. Andersson, Atomistic modeling of out-of-pile xenon diffusion by vacancy clusters in UO_2, J. Nucl. Mater. 520 (2019) 96–109.
[29] J.-P. Crocombette, Influence of charge states on energies of point defects and clusters in uranium dioxide, Phys. Rev. B 85 (2012) 144101.
[30] R. Konings, O. Benes, The heat capacity of NpO_2 at high temperatures: The effect of oxygen Frenkel pair formation, J. Phys. Chem. Solids 74 (2013) 653.
[31] D. Staicu, T. Wiss, V.V. Rondinella, J.P. Hiernaut, R.J.M. Konings, C. Ronchi, Impact of auto-irradiation on the thermophysical properties of oxide nuclear reactor fuels, J. Nucl. Mater. 397 (2010) 8.
[32] G.E. Murch, C.R.A. Catlow, Oxygen diffusion in UO_2, ThO_2 and PuO_2. A review, J. Chem. Soc. Faraday Trans. 83 (1987) 1157.
[33] K. Clausen, W. Hayes, J.E. Macdonald, R. Osborn, M.T. Hutchings, Observation of Oxygen Frenkel Disorder in Uranium Dioxide above 2000 K by Use of Neutron-Scattering Techniques, Phys. Rev. Lett. 52 (1984) 1238.
[34] E. Vathonne, J. Wiktor, M. Freyss, G. Jomard, M. Bertolus, DFT + *U* investigation of charged point defects and clusters in UO_2, J. Phys. Condens. Matter 26 (2014) 349601.
[35] Y. Miao, D. Aidhy, W.-Y. Chen, K. Mo, A. Oaks, D. Wolf, J. Stubbins, The evolution mechanism of the dislocation loops in irradiated lanthanum doped cerium oxide, J. Nucl. Mater. 445 (2014) 209.
[36] X.-Y. Liu, B.P. Uberuaga, D. Perez, A.F. Voter, New helium bubble growth mode at a symmetric grain-boundary in tungsten: accelerated molecular dynamics study, Mater. Res. Lett. 6 (9) (2018) 522–530.
[37] X.M. Bai, A.F. Voter, R.G. Hoagland, B.P. Uberuaga, Efficient annealing of radiation damage near grain boundaries via interstitial emission, Science 327 (2010) 1631.
[38] A. Stukowski, Visualization and analysis of atomistic simulation data with OVITO–the open visualization tool, Model. Simul. Mater. Sci.Eng. 18 (1) (2009) 015012.
[39] M.W.D. Cooper, S.T. Murphy, P.C.M. Fossati, M.J.D. Rushton, R.W. Grimes, Thermophysical and anion diffusion properties of $(U_x,Th_{1-x})O_2$, Proc. R. Soc. A 470 (2014) 20140427.
[40] Y.N. Osetsky, D.J. Bacon, A. Serra, B.N. Singh, S.I. Golubov, One-dimensional atomic transport by clusters of self-interstitial atoms in iron and copper, Philo. Mag. 83 (1) (2003) 61–91.